https://doi.org/10.1016/j.ijmecsci.2017.09.018

Numerical modeling and experimentation of three dimensional material removal characteristics in fluid jet polishing

C.J. Wang, C.F. Cheung*, M.Y. Liu

Partner State Key Laboratory of Ultra-precision Machining Technology, Department of Industrial and Systems Engineering, The Hong Kong Polytechnic University, Hung Hom, Kowloon, Hong Kong

Abstract: Fluid jet polishing is a promising ultra-precision polishing technology which has been successfully used in polishing various kinds of precision components. The characterization of the material removal plays an important role in deterministic ultra-precision polishing process, which not only helps to better understand its material removal characteristics, but is also used to predict the material removal and help to determine the dwell time needed at different positions of the workpiece. During the fluid jet polishing process, both vertical and oblique polishing modes are often used for different purposes. However, currently published researches about the modeling of fluid jet polishing are usually focused on the vertical impinging mode. Relatively few attentions have been paid to model the material removal in oblique impinging mode, whose material removal profile is asymmetric. As a result, this paper attempts to present a universal three dimensional numerical model (U3DNM) which can be used to model the fluid jet polishing process both in vertical and oblique impinging modes. The U3DMN is built based on the computational fluid dynamic modelling method. Four groups of simulations and polishing experiments were also conducted under various conditions so as to test the feasibility and reliability of this model. The results infer that the proposed numerical model is effective and has high robustness under various conditions. The successful development of the U3DNM provides a better understanding of the material removal characteristics which shed some light for better understanding and analysis of material removal for freeform surfaces which possesses continuous variation of curvatures.

Keywords: Fluid jet polishing; modeling; material removal; tool influence function; characterization; ultra-precision machining

1. Introduction

Fluid jet polishing (FJP) [1,2], as one of the promising ultra-precision deterministic polishing technology, has been successfully used in machining optical lenses, and replication molds made of a variety of difficult-to–machine-materials [3-6]. In FJP, abrasives and water are mixed adequately by mechanical stirring in a tank, and pumped at a low-pressure (normally between 4 bar and 20 bar [7]) to a nozzle as shown in Fig 1(a). The generated jet impinges the target surface leading to material removal, as shown in Fig. 1(b) and Fig. 1(c). Compared to traditional polishing methods, FJP has many advantages including the ability to polish various freeform surfaces, no tool wear during the polishing process, no temperature raise during the polishing process, the ability to generate small tool influence functions (TIF) to dramatically reduce the edge effect, and a wide range of material removal rates through controlling the polishing parameters. [2,7]

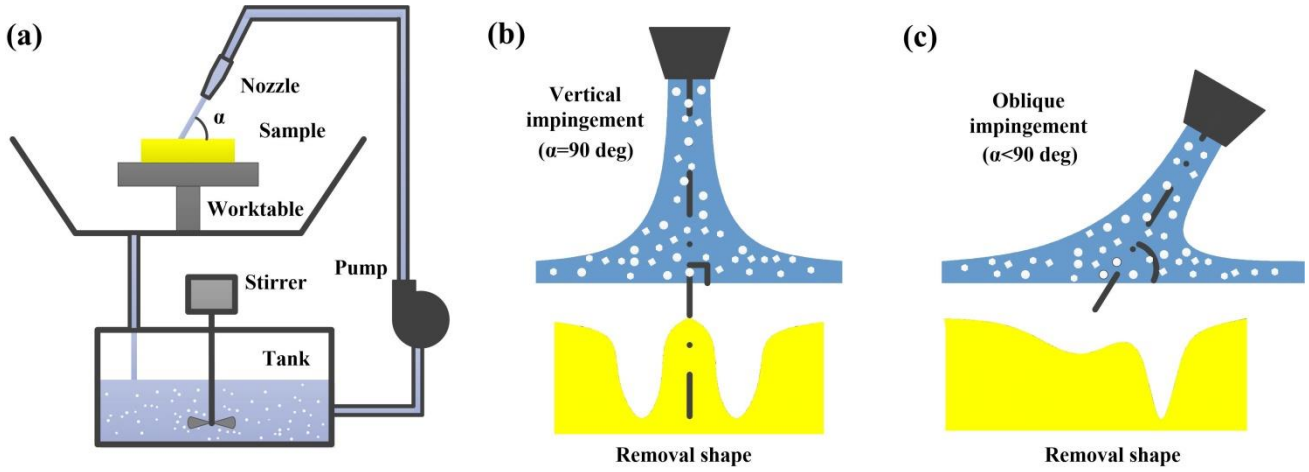

Fig. 1 Schematic diagram of fluid jet polishing system. (a) Illustration of the system, (b) vertical jet impingement and its material removal shape, and (c) oblique jet impingement and its material removal shape.

Deterministic polishing process, such as ion beam figuring [8,9], magnetorheological finishing [10,11], bonnet polishing [12,13], fluid jet polishing, etc., adopts a highly stabled TIF to move along a designated tool path so as to realize deterministic material removal. Its material removal process is represented by the two-dimensional convolution between the TIF and the dwell time. Hence, it is vital to build a precision model to compute the TIF. It is not only used to predict the surface generation, but also applied to optimize the combination of the polishing parameters. In recent years, a number of literatures have been published focused on the modeling of material removal characteristics or TIF. Liao et al. [14] built a mathematical model of the dynamic removal functions of ion beam figuring. Kordonski and Gorodkin [15] presented a material removal model of both magnetorheological finishing and magnetorheological jet finishing based on the principle of conservation of particles momentum in a binary suspension. Kim et al. [16], Cheung et al. [17], and Wang et al. [18] demonstrated a TIF model of bonnet tool polishing based on the Preston equation [19]. Moreover, a multi-scale theoretical model of bonnet tool polishing was also built recently by Cao and Cheung [20], based on the study of contact mechanics, kinematics theory and wear mechanism.

In abrasive waterjet machining, Liu et al. [21] and Anwar et al. [22] built their material removal models based on the finite element method, and Axinte et al. [23-25] adopted the mathematical method to model the material removal characteristics. However, the fluid pressure in FJP is much lower, leading to much slower abrasive velocity, and the material removal is quite different from that of high pressure abrasive waterjet machining. The TIF of the FJP was firstly investigated by Fähnle et al. [26] and Booij [2] experimentally at the beginning of the development of FJP. Shi et al. [27] established theoretical description for material removal spot shape of FJP in vertical impinging mode. However, the model is not tolerably accurate and further investigations are still needed to improve the model. Li et al. [28] used the k-ε turbulent model to compute the fluid propagation out of the nozzle. Considering that the k-ε turbulent model is not the best suitable model to simulate laminar to turbulent flow transitions as observed in FJP, Beaucamp et al. [7] adopted the shear-stress transport k-ω model instead to describe the slurry/air interface in the modeling of FJP, and this model was then successfully used to optimize surface texture performance down to 1nm arithmetic roughness (Ra) on electroless nickel plated optical dies.

Cao and Cheung [29] combined the computational dynamic fluid (CFD) model and single particle erosion model to describe the material removal characteristics in FJP. Recently, Qi et al. [30] developed a two dimensional CFD

model to investigate the effect of the machining parameters in ultra-sonic vibration assisted abrasive slurry jet machining. However, these models are mostly based on the computed data from the two dimensional CFD model, following with revolving data along the central axis to obtain the three dimensional data. They are useful when the impinging jet angle to the target surface is 90 degree. Nevertheless, they can hardly be used to model the situation when the jet is oblique to the surface. Hu [31] built the three dimensional material removal model of fluid jet polishing combining the CFD method and Huang's [32] erosion model. However, the material removal model in oblique impinging mode was not built and discussed. Oblique impinging jet polishing is usually accompanied with the vertical impinging jet polishing in the practical polishing process. The former one can help to get better surface roughness than the later one. Moreover, the Gaussian-like TIF of the fluid jet polishing is often generated from rotating the TIF of oblique jet polishing [28], or superimposing several TIFs of the oblique jet polishing [33]. Hence, the modeling of the oblique jet polishing also plays an important role in fluid jet polishing as well as the vertical jet polishing.

This paper presents a universal three dimensional numerical model of fluid jet polishing based on CFD method, which can be used to model both vertical jet polishing and oblique jet polishing. Simulations together with experimentations are also conducted under various conditions to validate this model.

2. Numerical modeling

2.1 Geometrical modeling

Figure 2 shows the geometric models of both vertical and oblique jet impingement. Conic-cylindrical type nozzle was used for the polishing process. Moreover, the detail parameters of the nozzle design have also been shown in Fig. 2. Hexahedral mesh built in ICEM CFD software package was adopted to enhance the simulation accuracy as shown in Fig. 3. The workpiece material is nickel copper alloy and BK7 glass. The 4000# Silicon Carbide (SiC) abrasive with an average diameter of 3.2 μm is used in this simulation.

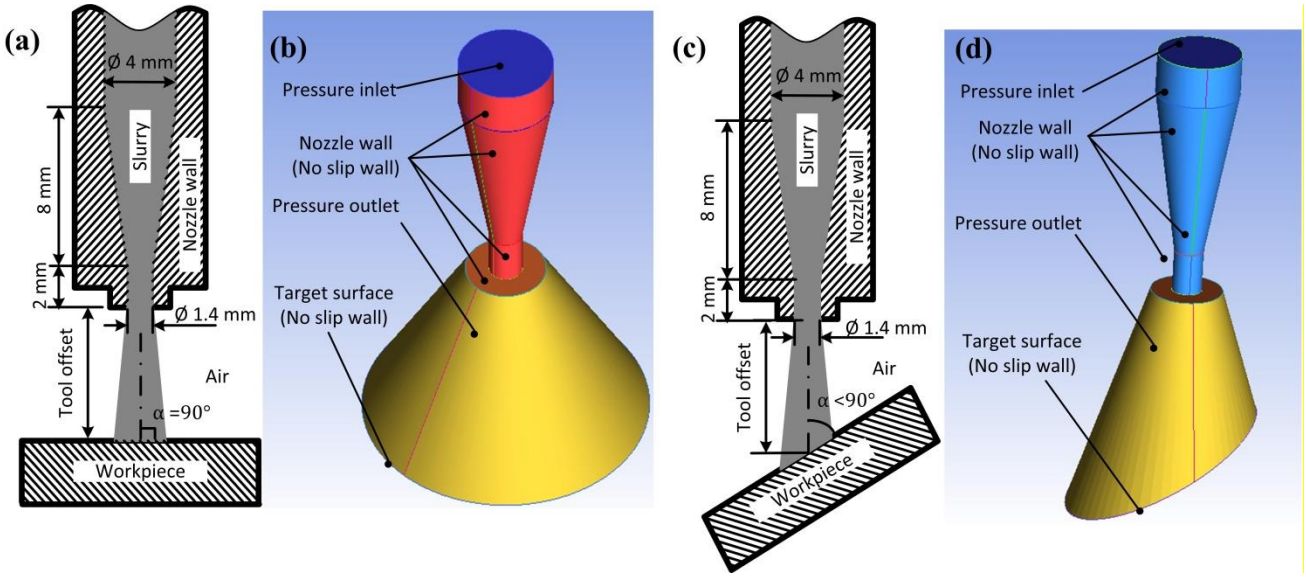

Fig. 2 Geometric models of fluid jet polishing with vertical and oblique impingement. (a) Practical model of vertical jet impingement, (b) simplified geometric model of vertical impingement for computational fluid dynamic simulation, (c) practical model of oblique jet

impingement, and (d) simplified geometric model of oblique impingement for computational fluid dynamic simulation. (α is the impinging angle.)

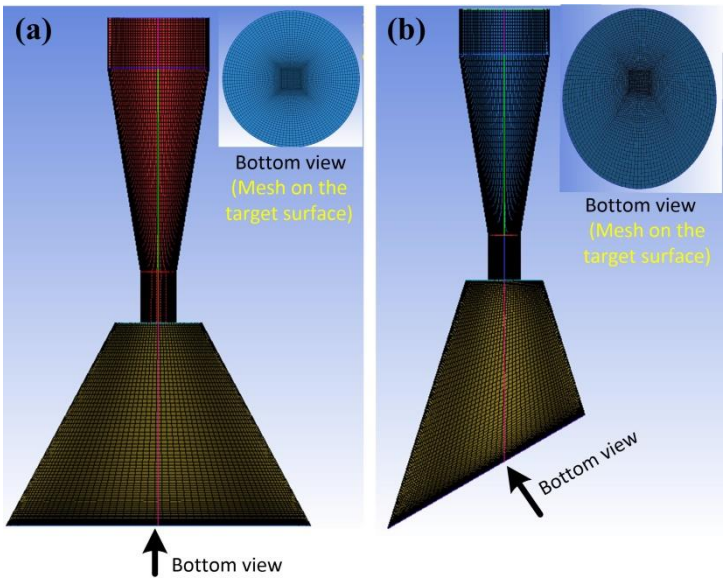

Fig. 3 Mesh models. (a) Vertical jet impingement, and (b) oblique jet impingement

2.2 Computational fluid dynamics method

The Eulerian-Lagrangian approach in the FLUENT software package was used to simulate the multiphase flow that involves liquid water, air, and abrasive particles. In the simulation, water and air were treated as Eulerian phases, while the abrasive particle was treated as Lagrangian phase. Several assumptions were made in this simulation process, which are: i) no abrasion of the nozzle during the polishing process; ii) the abrasive particle is assumed to have uniform size and shape; iii) the slurry concentration is constant during the polishing process; iv) the particle-particle interaction is neglected. In addition, ductile mode material removal is assumed in the fluid jet polishing process even in brittle materials considering the low fluid pressure.

2.2.1 Continuous phase model

In FJP, the assumption is made that the fluid flow is incompressible, and operates with constant density and temperature conditions. Hence, the incompressible form of the Navier-Stokes equation can be used in such case to describe the fluid velocity field [7]:

$$\rho\left(\frac{\partial v}{\partial t}+v\cdot\nabla v\right)=-\nabla p+\mu\nabla^2 v+f \tag{1}$$

where ρ is the fluid density, v the fluid velocity field, p the fluid pressure, μ the fluid viscosity, and f represents the external forces acting on the fluid.

For turbulence modeling, the Shear-Stress Transport (SST) based on a blending of the k-ω and k-ε turbulence models is used to express the turbulent fluid flow in the inner region of the boundary layer as well as in the outer art of the boundary layer for a wide range of the Reynolds number [34]. The superior performance of this model has been shown in the earlier studies [7,28,35]. SIMPLE algorithm [36] was employed to solve the pressure-velocity

coupling. Second-order upwind scheme and second-order central-differencing scheme are used for corrective and diffusion terms, respectively.

2.2.2 Discrete phase model

In this simulation, particle trajectories were computed using the discrete phase model (DPM) [36,37]. Lagrangian particle tracking is performed by considering the fluid forces acting on solid particle. The time variation of the particle velocity, v_p, is dependent on the forces acting on the particle, which can be expressed as

$$\frac{dv_p}{dt} = F_D\left(v - v_p\right) + \frac{g(\rho_p - \rho)}{\rho_p} + F \tag{2}$$

where ρ_p is the particle density, F_D is the drag force per unit particle mass, the second term in Eq. (2) is the gravity force and the third term (F) is an additional acceleration forces. The drag force, F_D is defined as

$$F_D = \frac{18\mu}{\rho_p d_p^2}\frac{C_D Re}{24} \tag{3}$$

where d_p is the abrasive particle diameter, Re is the relative Reynolds number, which is defined as follows:

$$Re = \frac{\rho_p d_p (v_p - v)}{\mu} \tag{4}$$

And C_D is the drag coefficient, evaluated using empirical formulation for non-spherical particle(angular), which is defined by Haider and Levenspiel [38].

For the computation of the discrete phase, the particle trajectories are numerically solved by stepwise integration over discrete time steps of Eq. (2) using stochastic tracking technique [36]. Stochastic tracking includes the effect of turbulent velocity fluctuations on the particle trajectories using discrete random walk model [39]. The effect of the discrete phase to the continuum phase is considered through adopting the two-way coupling method. Drag force is the dominant term in Eq. (2), which strongly depends on the Reynolds number of fluid flow and the difference in fluid flow and particle velocity. Other forces, such as gravity force, Brownian force, Saffman's lift force, pressure gradient force, and virtual mass force, are very small as compared to the drag force and thus neglected in this modeling study.

2.2.3 Particle rebound velocity model

The particle may collide with the wall surface and rebound back to the fluid flow domain when moving in the flow system. In this study, the rebound model developed by Grant and Tabakoff [40] is used to determine the particle trajectory and rebound velocity after impact [41]. In this model, the normal coefficient e_n and tangent coefficient e_t are expressed as

$$e_n = 0.993 - 1.76\theta - 1.56\theta^2 - 0.49\theta^3 \tag{5}$$

$$e_t = 0.988 - 1.66\theta + 2.11\theta^2 - 0.67\theta^3 \tag{6}$$

where θ is the impact angle in radians.

2.3 Erosion method

In fluid jet polishing, due to the low working pressure, the particle abrasives are dragged by the fluid flow at

smaller velocities and then impact the target surface as compared with abrasive water jet machining [12]. The resulting impact most probably erodes the surfaces made of hard and brittle materials in a ductile regime [29]. This erosion phenomenon also appears in many industrial situations, such as oil production and transportation, mineral processing and mining, and other slurry handling equipment. Hence, a wide variety of erosion models had been proposed in the past few decades. Finnie [42] developed a model at the first time for ductile materials. The model shows reasonable agreement with the experimental data for small impingement angle, while a poor agreement for large impingement angle. After that, Bitter [43,44] proposed an erosion model including two types of material removal: one is due to repeated deformation; the other is cutting wear. This model overcomes the limitations of Finnie's model. An extension of Finnie's work, the rigid-plastic theory developed by Hutchings et al. [45-47] predicted the collision kinematics and crater dimensions for single impacts of square and spherical particles on ductile targets. Papini and Spelt [48,49] presented and experimentally verified a rigid-plastic model of the erosion of ductile targets by the impact of single angular particles. Oka et al. [50,51] proposed an empirical model which can be used to estimate the erosion damage caused by solid particle impact. They claimed that this model can be utilized under any impact conditions and for any type of material. Zhang et al. [52] further tested Oka's model on different conditions, and the predicted results had good agreement with the experimental results.

In this study, Oka's model was employed to compute the eroded material, which involves the material properties of particle and sample as well as the impact conditions [53]. The erosion damage $E(\alpha)$ [mm^3/kg] can be written as

$$E(\alpha) = g(\alpha)E_{90} \tag{7}$$

where E_{90} is the erosion rate under normal particle impact, and $g(\alpha)$ denotes the impact angle dependence of the normalized erosion.

$$g(\alpha) = (\sin\alpha)^{n_1}\left(1 + Hv(1-\sin\alpha)\right)^{n_2} \tag{8}$$

$$n_1 = s_1(Hv)^{q_1}, n_2 = s_2(Hv)^{q_2} \tag{9}$$

$$E_{90} = K\left(Hv\right)^{k_1}(v_p)^{k_2}\left(d_p\right)^{k_3} \tag{10}$$

where n_1 and n_2 are exponents determined by the material hardness and other impact conditions, Hv [GPa] is an initial hardness number of the target surface. s_1, s_2, q_1, and q_2 are the fitting constants for the particle material. K denotes a particle property factor such as particle shape (angularity) and particle hardness, which has no correlation among different types of particles and other factors; k_1, k_2 and k_3 are exponent factors, which are affected by other parameters, respectively. As for SiC abrasive, k_2 can be expressed as [51]:

$$k_2 = 3.0(Hv)^{0.085} \tag{11}$$

Table 1 shows the value of the above coefficients and exponents adopted in this study while Table 2 summarizes the workpiece material properties used in this model. The erosion model was defined through a User Defined Function (UDF) in FLUENT software package. In ANSYS FLUENT software environment, the target surface erosion rate $R_{erosion}$ [kg/(m^{2}s)] is defined as [55]

$$R_{erosion} = \sum_{p=1}^{N_{particles}} \frac{\dot{m}_p ER}{A_{face}} \tag{12}$$

$$ER = 1.0\times10^{-9}\rho_w E\left(\theta\right) \tag{13}$$

where ER [kg/kg] is the erosion ratio, which is defined as the amount of mass loss of the target surface material due to particle impacts as divided by the mass of particles impacting; ρ_w [kg/m^3] is the density of the target surface material; A_{face} [m^2] is the area of the cell face at the wall; $\dot{m}_p$ [kg/s] represents the mass rate of particles impacting the cell surface. Hence, the erosion depth ED [m] after the dwell time T [s] can be computed by:

$$ED = \frac{R_{erosion}}{\rho_w} \cdot T \tag{14}$$

Then ED can be predicted directly in the FLUENT software through defining a custom defined function based on Eq. (14).

Table 1 Coefficients in the erosion model [50,51]

Coefficients	k_1	k_3	s_1	s_2	q_1	q_2
Value	-0.05	0.19	0.71	0.14	2.8	-1.00

Table 2 Material properties used in the simulation experiments [54]

Materials	Nickel copper alloy	BK7 glass	Silicon carbide abrasive
Density (kg/m3)	9091	2510	3100
Vicker's hardness (GPa)*	1.363	6.166	27.445

*Tested by Mitutoyo hardness testing machine.

3. Experimentation

To demonstrate the predictability of the numerical model, and validate its effectiveness, a series of simulation and polishing experiments were conducted under different polishing conditions and different materials.

3.1 Experimental setup

The experiments were conducted on a ZEEKO IRP 200 ultra-precision freeform polishing machine as shown in Fig. 4. The machine includes three linear axes (i.e. X-axis, Y-axis and Z-axis), three rotational axes (i.e. A-axis, B-axis, C-axis) and one spindle axis, i.e. H-axis. It can perform bonnet polishing and FJP, and has been successfully used to polish ultra-precision optical components such as optical moulds, etc. To test its robust performance, the simulation model was performed under various kinds of conditions, including different polishing conditions, different materials, and different impinging angles.

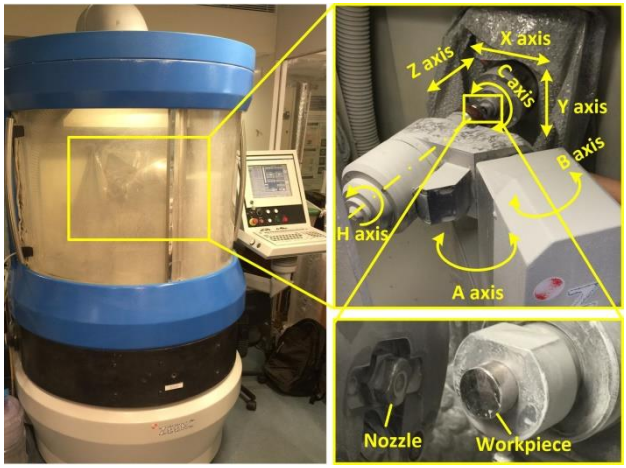

Fig. 4 Photographs of the experimental setup

3.2 Experimental design

Table 3 summarizes the experimental design. There were 4 groups of experiments to be conducted to assess the numerical model under different slurry pressure, different tool offsets, different materials, and different impinging angles, respectively. Both ductile and brittle materials were tested in this experiment design, which are nickel copper alloy (ductile material) and BK7 glass (brittle material), respectively. In addition, the nozzle diameter used in the experiment is 1.4mm, and the polishing slurry is ~5 wt.% silicon carbide mixed with pure water. Three spots were generated for each case in the experiment. The dwell time for each spot is 3 minutes. The generated spots were measured by a Zygo Nexview 3D optical profilometer.

Table 3 Experimental design under different polishing conditions

Polishing conditions		Impinging angle (°)	Workpiece material	Tool offset (mm)	Slurry pressure (bar)
Group A	A1	90	Nickel copper alloy	6	**4**
	A2	90	Nickel copper alloy	6	**6**
	A3	90	Nickel copper alloy	6	**8**
Group B	B1 (A3)	90	Nickel copper alloy	**6**	8
	B2	90	Nickel copper alloy	**7**	8
	B3	90	Nickel copper alloy	**8**	8
Group C	C1	90	**BK7 glass**	6	4
	C2	90	**BK7 glass**	6	6
	C3	90	**BK7 glass**	6	8
Group D	D1(A3)	**90**	Nickel copper alloy	6	8
	D2	**75**	Nickel copper alloy	6	8
	D3	**60**	Nickel copper alloy	6	8

4. Results and discussions

4.1 Assessment criteria

Fig. 5 shows the simulation results of the two selective cases which are vertical impinging (Case A3) and oblique impinging (Case D3), respectively. For vertical impinging, the fluid flow uniformly spreads to all directions after impinging, leading to rotational symmetric erosion depth distribution. However, the fluid flow motion feature is no longer rotational symmetric, which leads to non-rotational symmetric erosion as shown in Fig. 5(d). In order to verify the effectiveness of the numerical model, the TIF shape was compared using a surface matching method. In a traditional matching method such as ICP (iterative closest point) [56], since the numerical model and the measured result have considerable large deviation and the deviation is distributed unevenly in directions, this will cause a large rotational matching error which is obviously unacceptable. Thus, the numerical model and the measurement data are compared through a matching algorithm based on the Gaussian process and image registration method [57], which considers three translational transforms in the registration process, to address the large rotational error issue caused by the uneven distributed deviation. As shown in Fig. 6, the matching process was demonstrated based on the results of two selective cases as shown in Fig. 5. Two independent 3D contours of the simulation and experiment results were matched in one figure, which can present their deviation directly. Moreover, their deviation value can be deduced through the subtraction of these two matched data. In this paper, the deviation of them was adopted as one of the assessment criteria for this numerical model. In addition, the peak-to-valley (*PV*) value of the TIF was also taken to quantitatively compare the material removal rate between the simulation and experiment results.

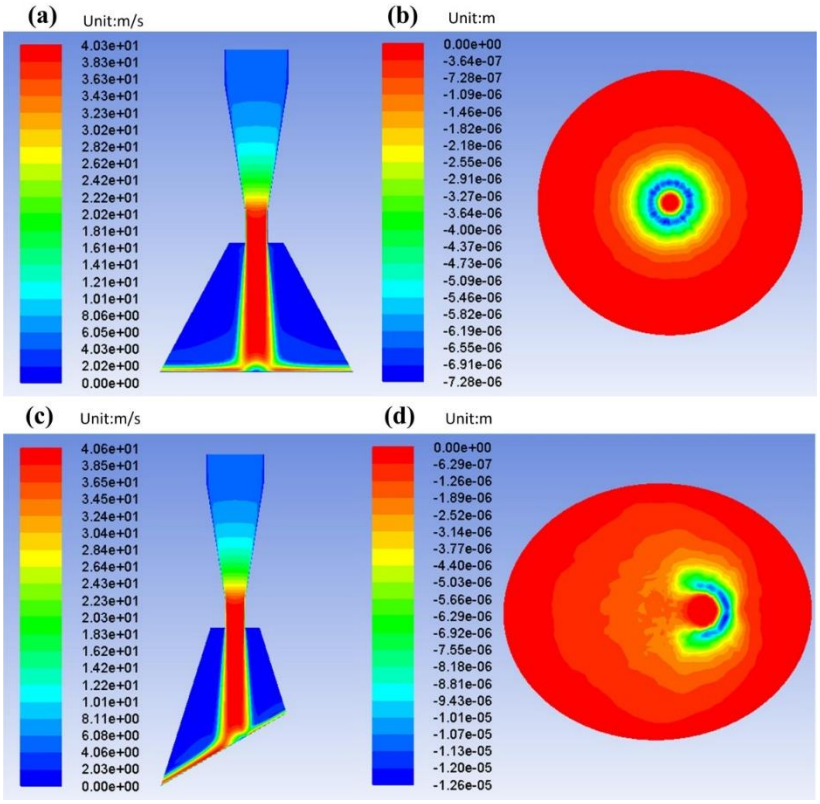

Fig. 5. CFD simulation results of two selective cases: (a) fluid velocity distribution in Case A3, (b) erosion depth distribution on the target surface in Case A3, (c) fluid velocity distribution in D3, and (d) erosion depth distribution on the target surface in Case D3.

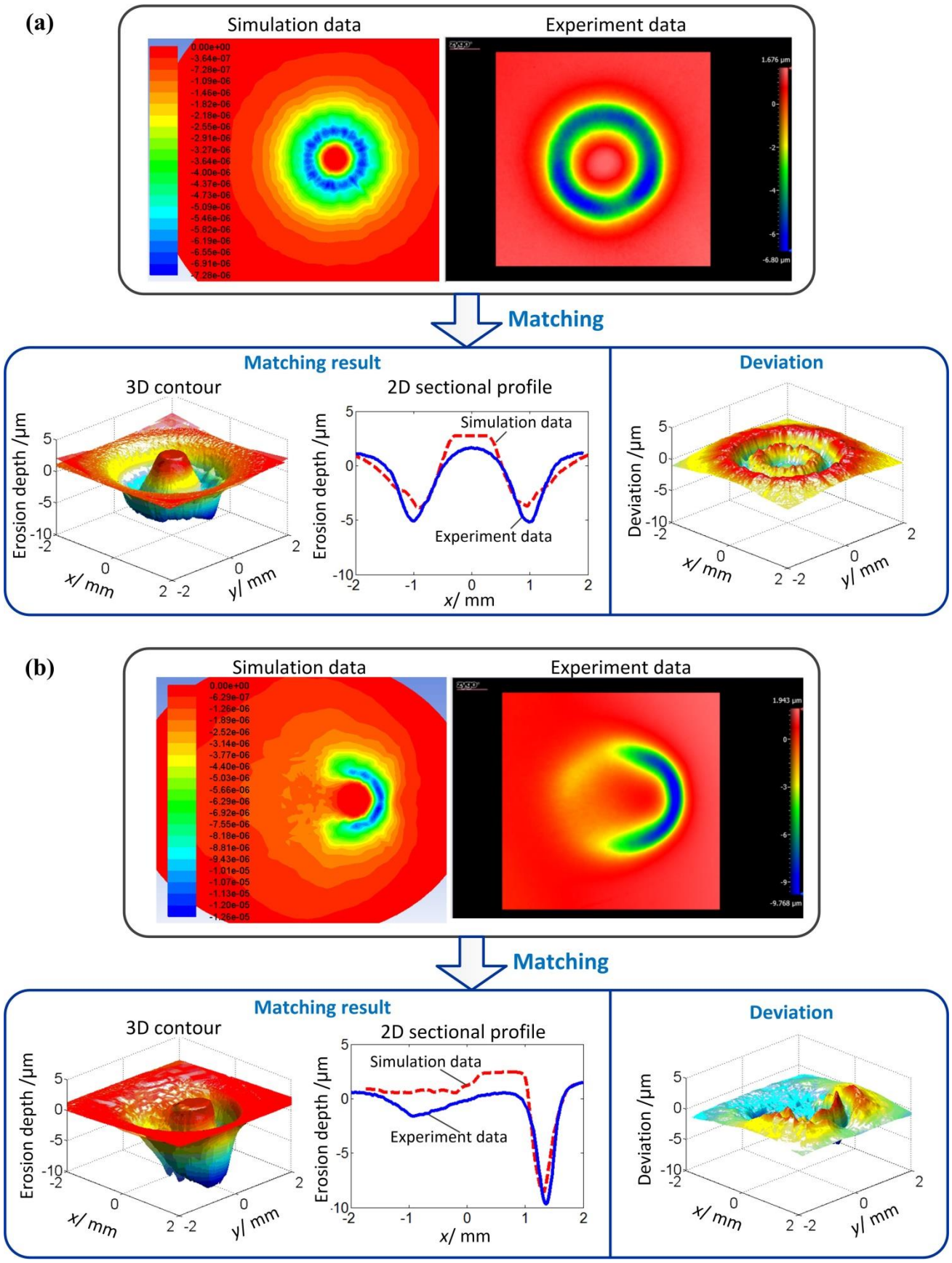

Fig. 6. TIF shape comparison of the simulation and experiment results through data matching in two selective cases: (a) Case A3, and (b) Case D3.

4.2 Comparison results and discussions

Fig. 7 shows the deviation results of these four groups of experiments, and the corresponding root-mean-square value were also calculated and displayed in each sub-figure. The predicted TIFs shape agree reasonably well with the measured experimental TIFs under various polishing conditions, including different tool offset, fluid pressure, workpiece material and impinging angle. It indicates that the proposed numerical model can be used to adequately predict the material removal profile in fluid jet polishing. It is interesting to note that there exists certain deviation between the predicted shapes and the experiment results. Theoretically, it may be caused by the assumptions made during the numerical computation, including the negligence of the particle-particle interaction, assumption of the uniform particle shape, uniform particle size, and non-abrasion of the nozzle, etc. Besides, the initial form error of the workpiece, and the stability of the slurry concentration could also attribute to the deviation. As a result, it is not surprising to find the deviation between the predicted TIFs and measured TIFs.

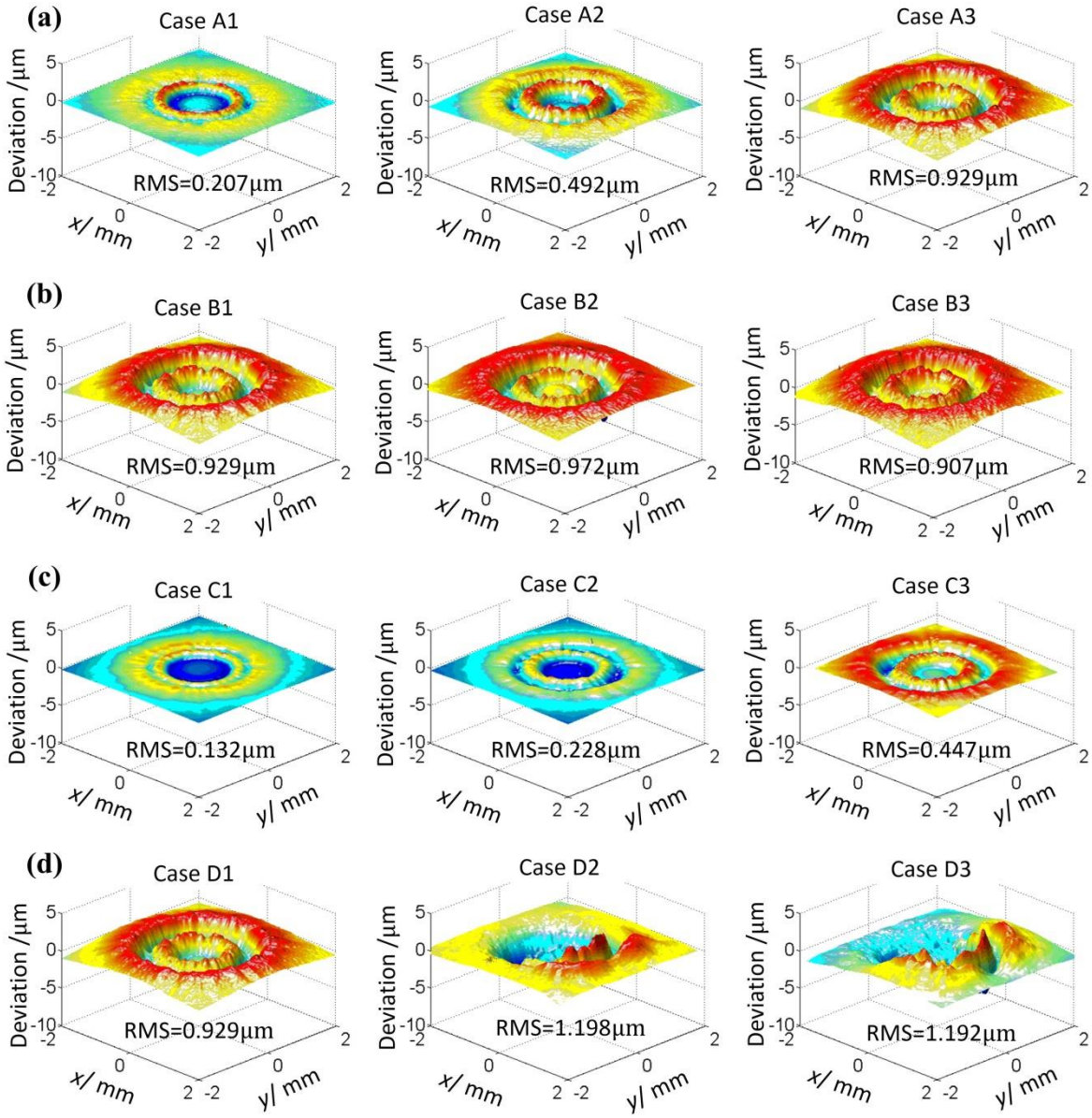

Fig. 7. Deviation results in the TIF shape comparison of these four groups: (a) group A, (b) group B, (c) group C, and (d) group D.

Fig. 8 shows the comparison of *PV* between the simulation and experiment results. It turns out that the simulation results show a reasonably good agreement with the experiment results. To further describe quantitatively the deviation between the simulation and the experimental results, the deviation ratio η defined in the Equation (15) has also been determined for each case.

$$\eta = \frac{\left|PV_{SIM} - PV_{EX-AVG}\right|}{PV_{SIM}} \times 100\% \tag{15}$$

where PV_{SIM} is the *PV* value of the simulated TIF, $PV_{EX\text{-}AVG}$ is the average *PV* value of the measured TIF. And the calculated η of each case has also been shown in Fig. 8. The value of η varies from 2.6% to 42.0%, and the average value of η in these 12 cases is 15.6%. The deviation is found to be as good as the results in Cao's [29] model or even smaller.

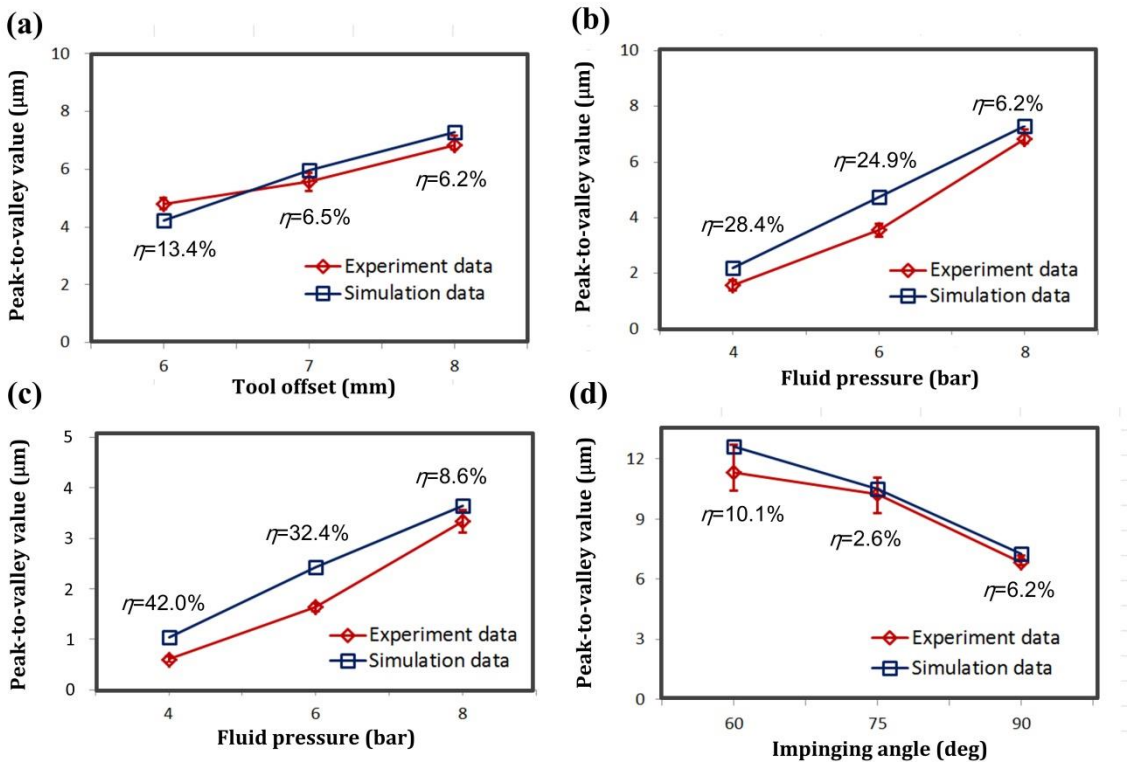

Fig. 8. Quantitatively comparison of peak-to-valley value of TIFs generated in these four groups: (a) group A, (b) group B, (c) group C, and (d) group D.

Besides, the predicted trends in terms of tool offset, fluid pressure, and impinging angle are consistent with the experimental results in this study. Hence, it further validates the robustness of the proposed numerical model for fluid jet polishing. It is also interesting to note that almost all the PV values of the simulation results are slightly larger than the experimental results. The reason may be due to the fact that the particle could become dull or worn out in practical polishing process which cause the decrease of its erosion rate, which is not considered in the numerical model.

5 Conclusions

To solve the modeling problem of oblique impinging situation in fluid jet polishing, a universal three dimensional numerical model was built based on Eulerian-Lagrangian approach combined with Oka's erosion model, which can be used to characterize the material removal both in vertical impinging and oblique impinging modes. This model has been validated through the comparison of the simulation and experiment results under different fluid pressure, tool offsets, impinging angles, and on both ductile and brittle materials. The results of the simulation and experiment were assessed in two aspects, which are the profile of the material removal shape and material removal rate, respectively. The assessment results demonstrate the effectiveness of the proposed model and high robustness under various conditions. This model can not only help to better understand the material removal characteristics in fluid jet polishing, but also can be used to accurately predict the material removal and dwell time computation in fluid jet polishing.

Acknowledgement

The work described in this paper was mainly supported by the Innovation and Technology Fund (grant number GHP/031/13SZ) from the Government of the Hong Kong Special Administrative Region, China. The work was also supported by PhD studentship (project code: RTHC) from The Hong Kong Polytechnic University.

References

[1]. Fähnle OW, Van Brug H, Frankena HJ. Fluid jet polishing of optical surfaces. Applied Optics 1998;37(28):6771-3.

[2]. Booij SM. Fluid Jet Polishing: Possibilities and limitations of a new fabrication technique. PhD Thesis 2003; Technical University of Delft.

[3]. Beaucamp A, Namba Y. Super-smooth finishing of diamond turned hard X-ray molding dies by combined fluid jet and bonnet polishing. CIRP Annals-Manufacturing Technology. 2013;62(1):315-8.

[4]. Zhu HT, Huang CZ, Wang J, Li QL, Che CL. Experimental study on abrasive waterjet polishing for hard–brittle materials. International Journal of Machine Tools and Manufacture. 2009;49(7):569-78.

[5]. Tsai FC, Yan BH, Kuan CY, Huang FY. A Taguchi and experimental investigation into the optimal processing conditions for the abrasive jet polishing of SKD61 mold steel. International Journal of Machine Tools and Manufacture. 2008;48(7):932-45.

[6]. Li ZZ, Wang JM, Peng XQ, Ho LT, Yin ZQ, Li SY, Cheung CF. Removal of single point diamond-turning marks by abrasive jet polishing. Applied optics. 2011;50(16):2458-63.

[7]. Beaucamp A, Namba Y, Freeman R. Dynamic multiphase modeling and optimization of fluid jet polishing process. CIRP Annals-Manufacturing Technology. 2012;61(1):315-8.

[8]. Wilson SR, Reicher DW, McNeil JR. Surface figuring using neutral ion beams. In 32nd Annual Technical Symposium 1989 Jan 29 (pp. 74-81). International Society for Optics and Photonics.

[9]. Xie X, Zhou L, Dai Y, Li S. Ion beam machining error control and correction for small scale optics. Applied Optics. 2011;50(27):5221-7.

[10]. Shorey AB, Kordonski WI, Gorodkin SR, Jacobs SD, Gans RF, Kwong KM, Farny CH. Design and testing of a new magnetorheometer. Review of Scientific Instruments. 1999;70(11):4200-6.

[11]. Tricard M, Kordonski WI, Shorey AB, Evans C. Magnetorheological jet finishing of conformal, freeform and steep concave optics. CIRP Annals-Manufacturing Technology. 2006;55(1):309-12.

[12]. Walker DD, Brooks D, King A, Freeman R, Morton R, McCavana G, Kim SW. The 'Precessions' tooling for polishing and figuring flat, spherical and aspheric surfaces. Optics Express. 2003;11(8):958-64.

[13]. Beaucamp A, Namba Y, Inasaki I, Combrinck H, Freeman R. Finishing of optical moulds to λ/20 by automated corrective polishing. CIRP Annals-Manufacturing Technology. 2011;60(1):375-8.

[14]. Liao W, Dai Y, Xie X, Zhou L. Mathematical modeling and application of removal functions during deterministic ion beam figuring of optical surfaces. Part 1: Mathematical modeling. Applied optics. 2014;53(19):4266-74.

[15]. Kordonski W, Gorodkin S. Material removal in magnetorheological finishing of optics. Applied Optics. 2011;50(14):1984-94.

[16]. Kim DW, Kim SW. Static tool influence function for fabrication simulation of hexagonal mirror segments for extremely large telescopes. Optics Express. 2005;13(3):910-7.

[17]. Cheung CF, Kong LB, Ho LT, To S. Modelling and simulation of structure surface generation using computer controlled ultra-precision polishing. Precision Engineering. 2011;35(4):574-90.

[18]. Wang C, Wang Z, Yang X, Sun Z, Peng Y, Guo Y, Xu Q. Modeling of the static tool influence function of bonnet polishing based on FEA. The International Journal of Advanced Manufacturing Technology. 2014;74(1-4):341-9.
[19]. Preston FW. The theory and design of plate glass polishing machines. J. Soc. Glass Tech. 1927;11:214.
[20]. Cao ZC, Cheung CF. Multi-scale modeling and simulation of material removal characteristics in computer-controlled bonnet polishing. International Journal of Mechanical Sciences. 2016;106:147-56.
[21]. Liu H, Wang J, Kelson N, Brown RJ. A study of abrasive waterjet characteristics by CFD simulation. Journal of Materials Processing Technology. 2004;153:488-93.
[22]. Anwar S, Axinte DA, Becker AA. Finite element modelling of abrasive waterjet milled footprints. Journal of Materials Processing Technology. 2013;213(2):180-93.
[23]. Axinte DA, Srinivasu DS, Billingham J, Cooper M. Geometrical modelling of abrasive waterjet footprints: a study for 90 jet impact angle. CIRP Annals-Manufacturing Technology. 2010;59(1):341-6.
[24]. Kong MC, Anwar S, Billingham J, Axinte DA. Mathematical modelling of abrasive waterjet footprints for arbitrarily moving jets: part I—single straight paths. International Journal of Machine Tools and Manufacture. 2012;53(1):58-68.
[25]. Billingham J, Miron CB, Axinte DA, Kong MC. Mathematical modelling of abrasive waterjet footprints for arbitrarily moving jets: part II—overlapped single and multiple straight paths. International Journal of Machine Tools and Manufacture. 2013;68:30-9.
[26]. Fähnle OW. Shaping and finishing of aspherical optical surfaces. PhD Thesis 1998; Technical University of Delft.
[27]. Shi C, Yuan J, Wu F, Hou X, Wan Y. Material removal model of vertical impinging in fluid jet polishing. Chinese optics letters. 2010;8(3):323-5.
[28]. Li Z, Li S, Dai Y, Peng X. Optimization and application of influence function in abrasive jet polishing. Applied Optics. 2010;49(15):2947-53.
[29]. Cao ZC, Cheung CF. Theoretical modelling and analysis of the material removal characteristics in fluid jet polishing. International Journal of Mechanical Sciences. 2014;89:158-66.
[30]. Qi H, Wen D, Lu C, Li G. Numerical and experimental study on ultrasonic vibration-assisted micro-channelling of glasses using an abrasive slurry jet. International Journal of Mechanical Sciences. 2016;110:94-107.
[31]. Hu S. Simulation and Verification of Fluid Jet Polishing. PhD thesis 2016; University of South Florida.
[32]. Huang C, Chiovelli S, Minev P, Luo J, Nandakumar K. A comprehensive phenomenological model for erosion of materials in jet flow. Powder Technology. 2008;187(3):273-9
[33]. Fang H, Guo P, Yu J. Surface roughness and material removal in fluid jet polishing. Applied optics. 2006;45(17):4012-9.
[34]. Menter FR. Two-equation eddy-viscosity turbulence models for engineering applications. AIAA journal. 1994;32(8):1598-605.
[35]. Zhang Z, Kleinstreuer C. Low-Reynolds-number turbulent flows in locally constricted conduits: a comparison study. AIAA journal. 2003;41(5):831-40.
[36]. Ansys Fluent, 12.0/12.1 Documentation, Users Guide Manual, Ansys Inc, 2009.
[37]. Mansouri A, Arabnejad H, Shirazi SA, McLaury BS. A combined CFD/experimental methodology for erosion prediction. Wear. 2015;332:1090-7.
[38]. Haider A, Levenspiel O. Drag coefficient and terminal velocity of spherical and nonspherical particles. Powder Technology. 1989;58(1):63-70.
[39]. Gosman AD, Loannides E. Aspects of computer simulation of liquid-fueled combustors. Journal of Energy.

1983;7(6):482-90.
[40]. Grant G, Tabakoff W. Erosion prediction in turbomachinery resulting from environmental solid particles. Journal of Aircraft. 1975;12(5):471-8.
[41]. Nguyen VB, Nguyen QB, Liu ZG, Wan S, Lim CY, Zhang YW. A combined numerical–experimental study on the effect of surface evolution on the water–sand multiphase flow characteristics and the material erosion behavior. Wear. 2014;319(1):96-109.
[42]. Finnie I. Erosion of surfaces by solid particles. Wear. 1960;3(2):87-103.
[43]. Bitter JG. A study of erosion phenomena part I. Wear. 1963;6(1):5-21.
[44]. Bitter JG. A study of erosion phenomena: Part II. Wear. 1963;6(3):169-90.
[45]. Hutchings IM, Winter RE, Field JE. Solid particle erosion of metals: the removal of surface material by spherical projectiles. InProceedings of the Royal Society of London A: Mathematical, Physical and Engineering Sciences 1976 Mar 9 (Vol. 348, No. 1654, pp. 379-392). The Royal Society.
[46]. Hutchings IM. Deformation of metal surfaces by the oblique impact of square plates. International Journal of Mechanical Sciences. 1977;19(1):45IN747-6IN852.
[47]. Hutchings IM, Macmillan NH, Rickerby DG. Further studies of the oblique impact of a hard sphere against a ductile solid. International Journal of Mechanical Sciences. 1981;23(11):639-46.
[48]. Papini M, Spelt JK. Impact of rigid angular particles with fully-plastic targets Part I: Analysis. International Journal of Mechanical Sciences. 2000;42(5):991-1006.
[49]. Papini M, Spelt JK. Impact of rigid angular particles with fully-plastic targets Part II: Parametric study of erosion phenomena. International Journal of Mechanical Sciences. 2000;42(5):1007-25.
[50]. Oka YI, Okamura K, Yoshida T. Practical estimation of erosion damage caused by solid particle impact: Part 1: Effects of impact parameters on a predictive equation. Wear. 2005;259(1):95-101.
[51]. Oka YI, Yoshida T. Practical estimation of erosion damage caused by solid particle impact: Part 2: Mechanical properties of materials directly associated with erosion damage. Wear. 2005;259(1):102-9.
[52]. Zhang Y, Reuterfors EP, McLaury BS, Shirazi SA, Rybicki EF. Comparison of computed and measured particle velocities and erosion in water and air flows. Wear. 2007;263(1):330-8.
[53]. Wang CJ, Cheung CF, Ho LT, Liu MY, Lee WB. A novel multi-jet polishing process and tool for high-efficiency polishing. International Journal of Machine Tools and Manufacture. 2017;115:60-73.
[54]. http://www.matweb.com/
[55]. ANSYS FLUENT Theory Guide, Release 14.0, Ansys Inc., 2011.
[56]. Besl PJ, McKay ND. A method for registration of 3-D shapes. IEEE Transactions on pattern analysis and machine intelligence. 1992;14:239-56.
[57]. Liu MY, Cheung CF, Cheng CH, Su R, Leach RK. A Gaussian process and image registration based stitching method for high dynamic range measurement of precision surfaces. Precision Engineering. 2017.(published online) https://doi.org/10.1016/j.precisioneng.2017.04.017